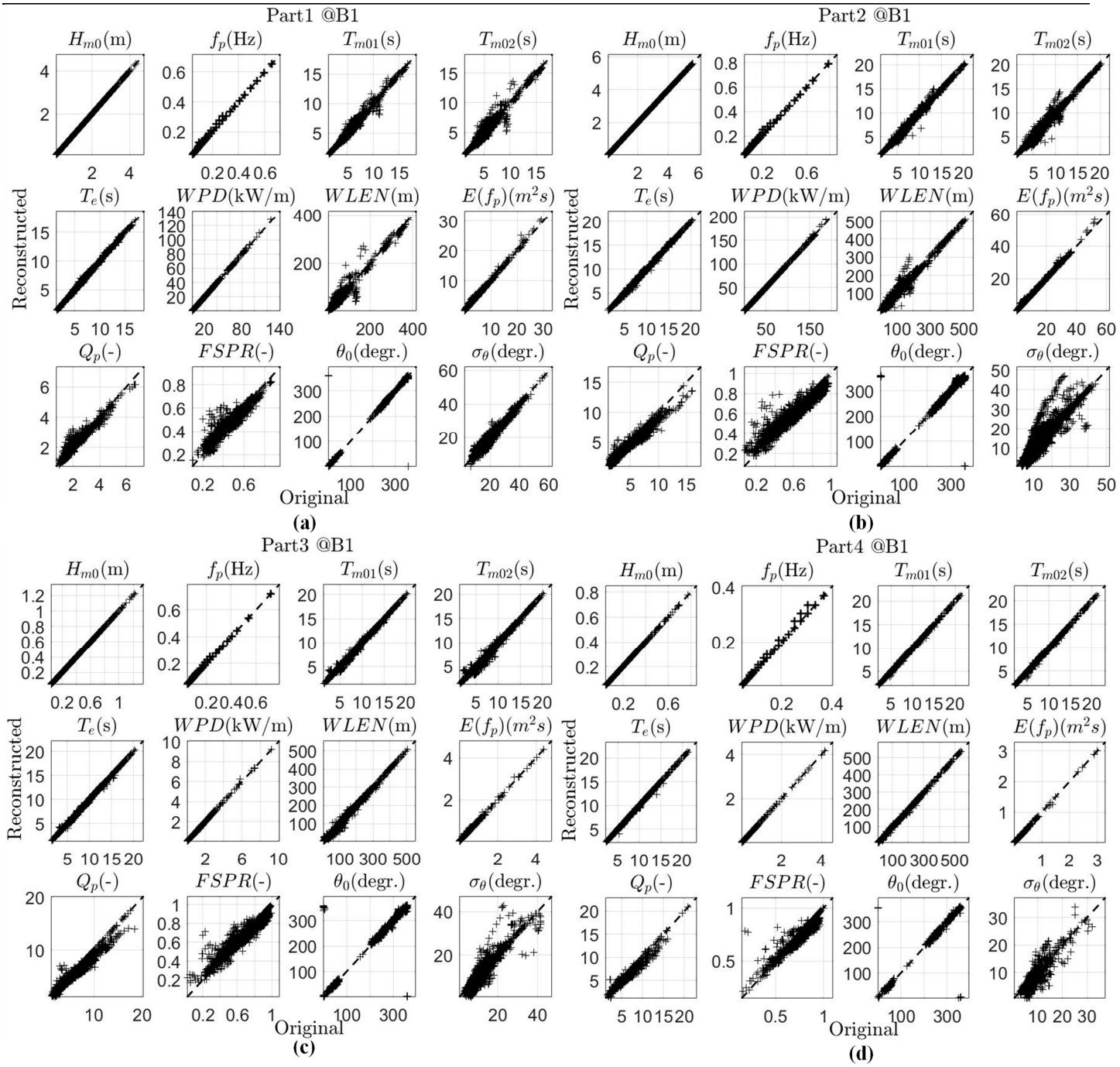

Figure S1. Scatter plots for KPs obtained from the original and the reconstructed partitions at check point B1: (a) Partition 1, (b) Partition 2, (c) Partition 3, and (d) Partition 4. The partitions from the same spectrum are ordered from large to small based on their H_{m0} values.

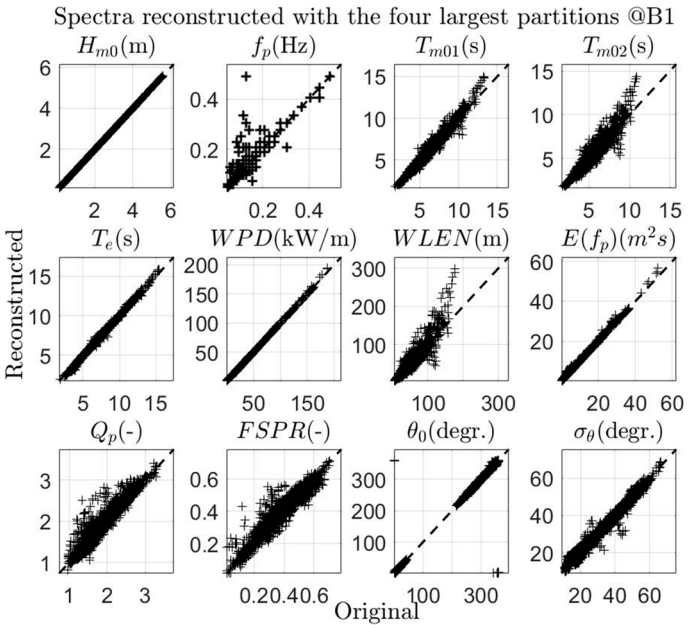

Figure S2. Scatter plots for KPs obtained from the original and the reconstructed spectra (with the four largest partitions) at check point B1.

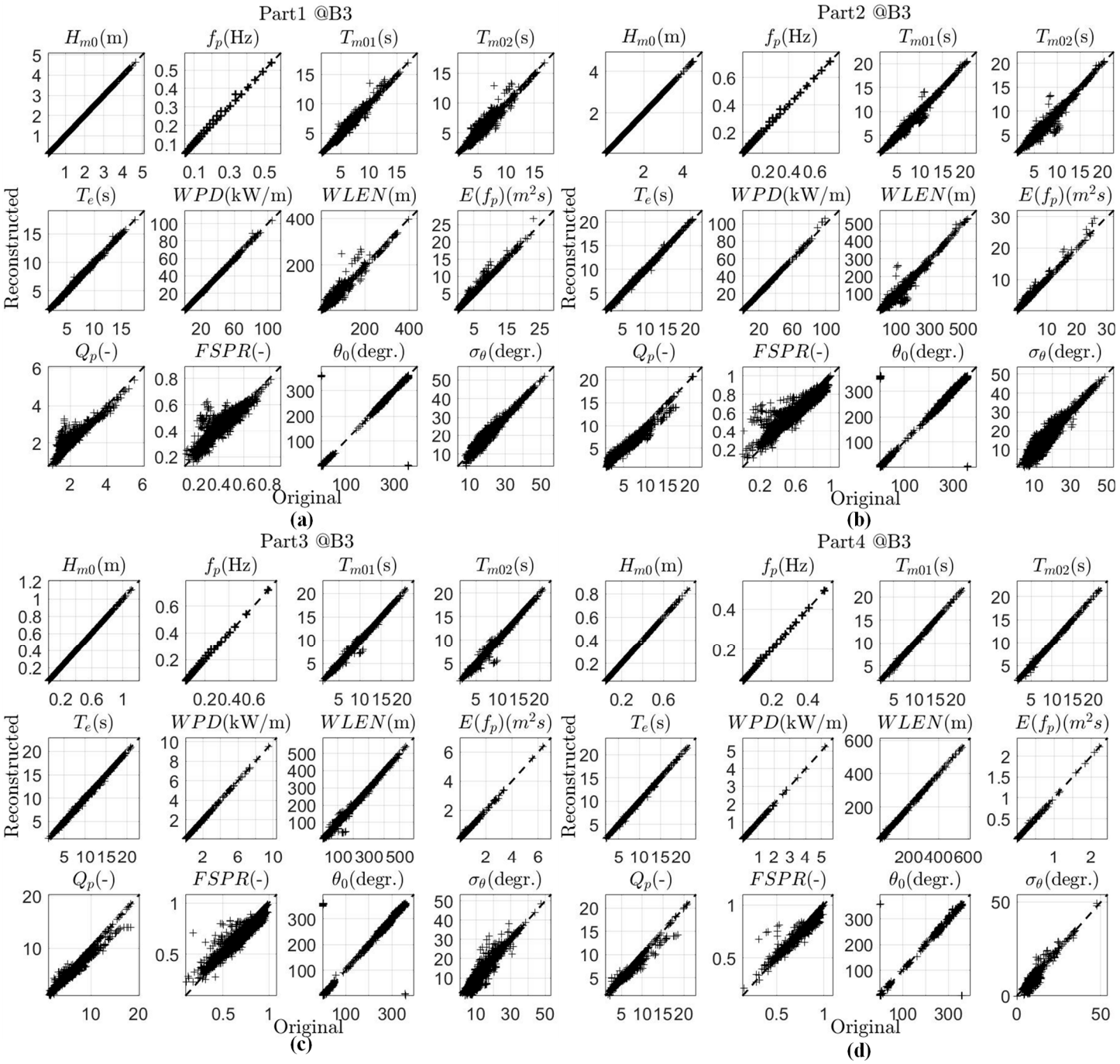

Figure S3. Scatter plots for KPs obtained from the original and the reconstructed partitions at check point B3: (a) Partition 1, (b) Partition 2, (c) Partition 3, and (d) Partition 4. The partitions from the same spectrum are ordered from large to small based on their H_{m0} values.

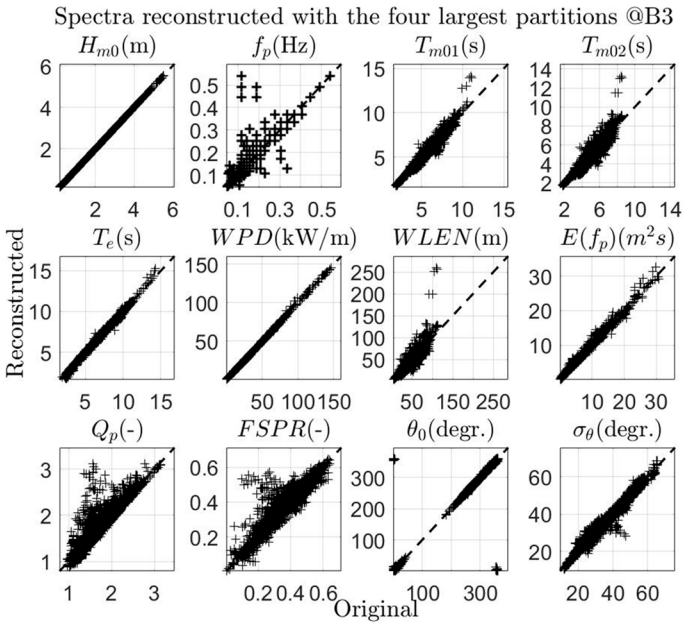

Figure S4. Scatter plots for KPs obtained from the original and the reconstructed spectra (with the four largest partitions) at check point B3.

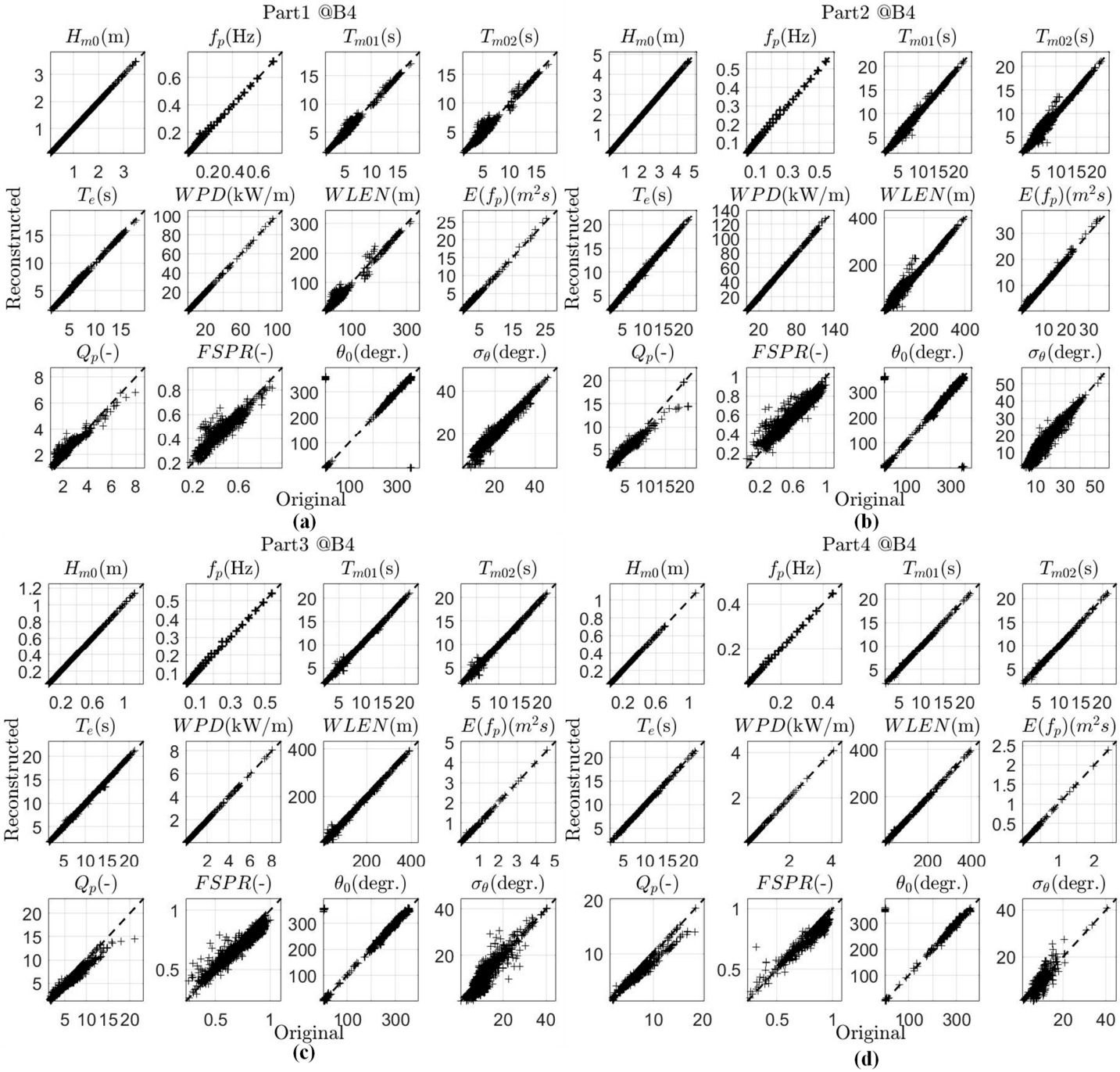

Figure S5. Scatter plots for KPs obtained from the original and the reconstructed partitions at check point B4: (a) Partition 1, (b) Partition 2, (c) Partition 3, and (d) Partition 4. The partitions from the same spectrum are ordered from large to small based on their H_{m0} values.

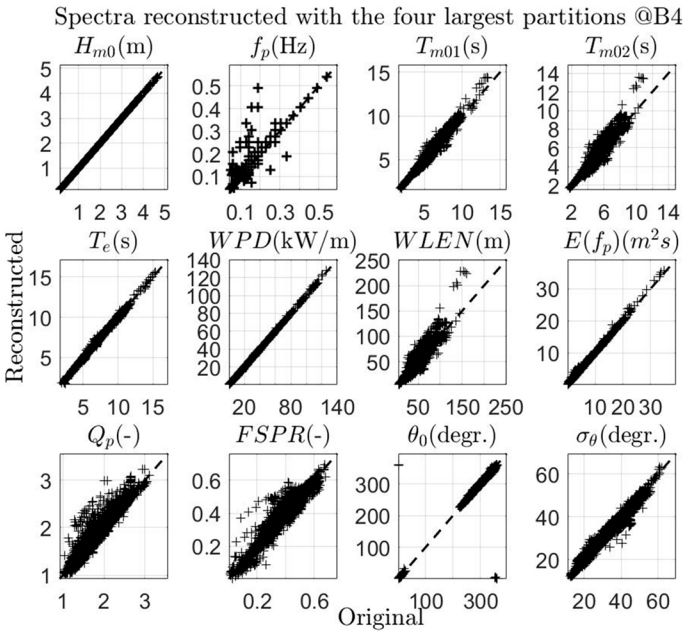

Figure S6. Scatter plots for KPs obtained from the original and the reconstructed spectra (with the four largest partitions) at check point B4.

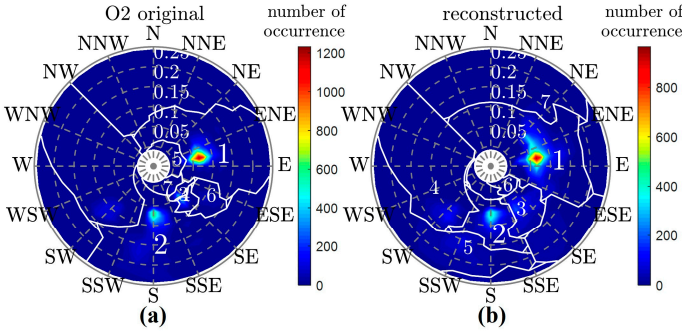

Figure S7. Groups identified at check point O2: **(a)** partition groups identified from the simulation with original boundaries, and **(b)** partition groups identified from the simulation with reconstructed boundaries. The $f-\theta$ spectral space is presented in polar coordinates, the number of occurrences of partition peaks in each $f-\theta$ cell is indicated by the colors, groups labeled 1–7 are ordered from large to small based on the peak-occurrence number, and the boundaries of the groups are depicted by the white lines.

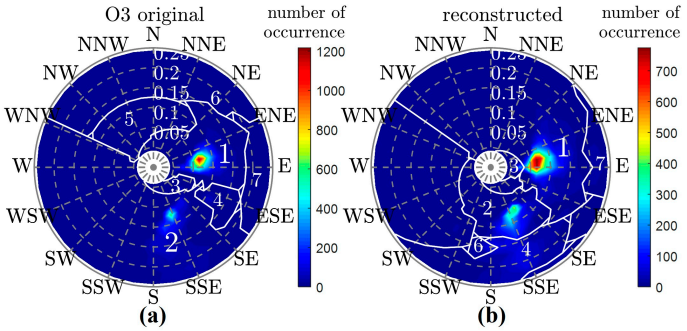

Figure S8. Groups identified at check point O3: **(a)** partition groups identified from the simulation with original boundaries, and **(b)** partition groups identified from the simulation with reconstructed boundaries. The $f-\theta$ spectral space is presented in polar coordinates, the number of occurrences of partition peaks in each $f-\theta$ cell is indicated by the colors, groups labeled 1–7 are ordered from large to small based on the peak-occurrence number, and the boundaries of the groups are depicted by the white lines.

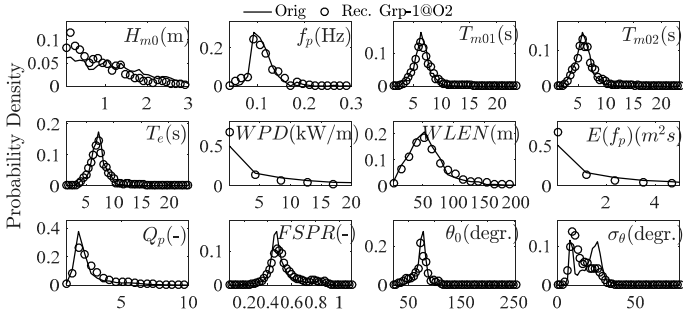

Figure S9. Probability distribution of partition KPs in Grp-1 at check point O2. Probability densities derived from spectra simulated with the original and the reconstructed boundaries are indicated by solid lines and circles, respectively. Each panel is titled according to the corresponding KP, and the x axis in each panel denotes the value range of the KP.

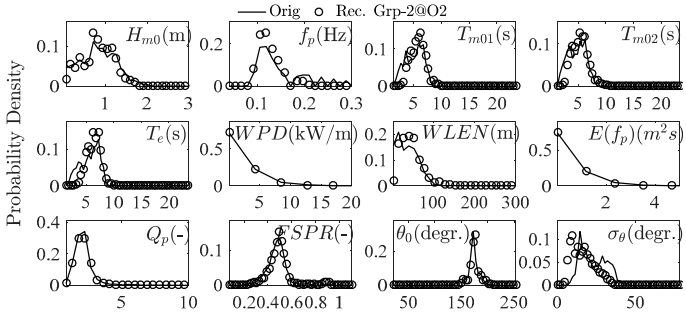

Figure S10. Probability distribution of partition KPs in Grp-2 at check point O2. Probability densities derived from spectra simulated with the original and the reconstructed boundaries are indicated by solid lines and circles, respectively. Each panel is titled according to the corresponding KP, and the x axis in each panel denotes the value range of the KP.

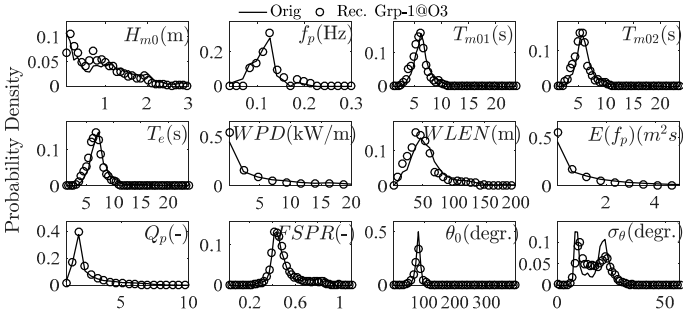

Figure S11. Probability distribution of partition KPs in Grp-1 at check point O3. Probability densities derived from spectra simulated with the original and the reconstructed boundaries are indicated by solid lines and circles, respectively. Each panel is titled according to the corresponding KP, and the x axis in each panel denotes the value range of the KP.

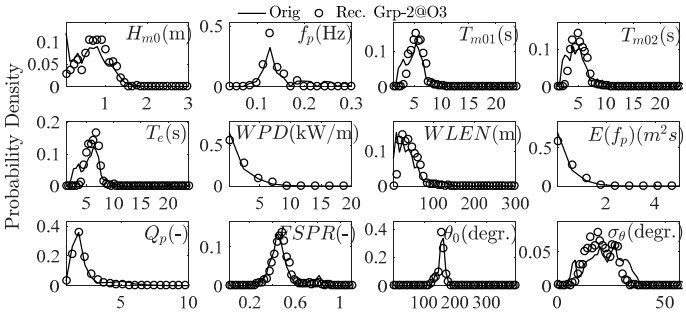

Figure S12. Probability distribution of partition KPs in Grp-2 at check point O3. Probability densities derived from spectra simulated with the original and the reconstructed boundaries are indicated by solid lines and circles, respectively. Each panel is titled according to the corresponding KP, and the x axis in each panel denotes the value range of the KP.

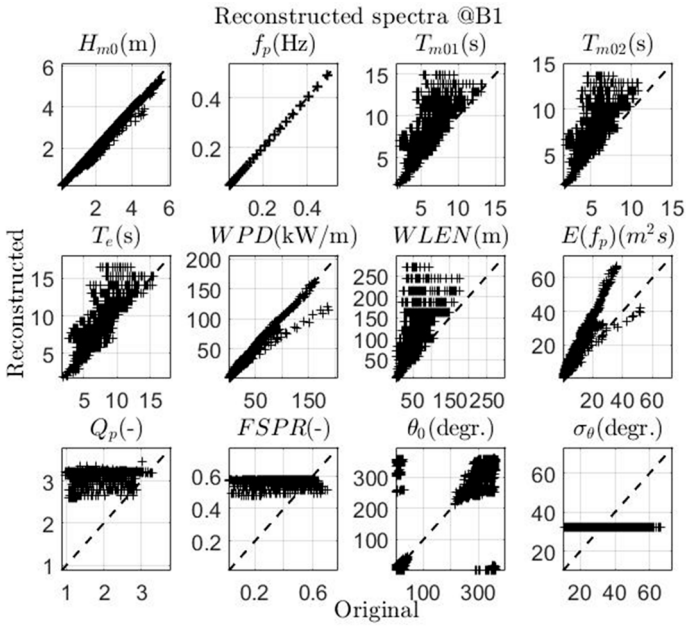

Figure S13. Scatter plots for KPs obtained from the original and the TMA–Mitsuyasu reconstructed spectra at check point B1.

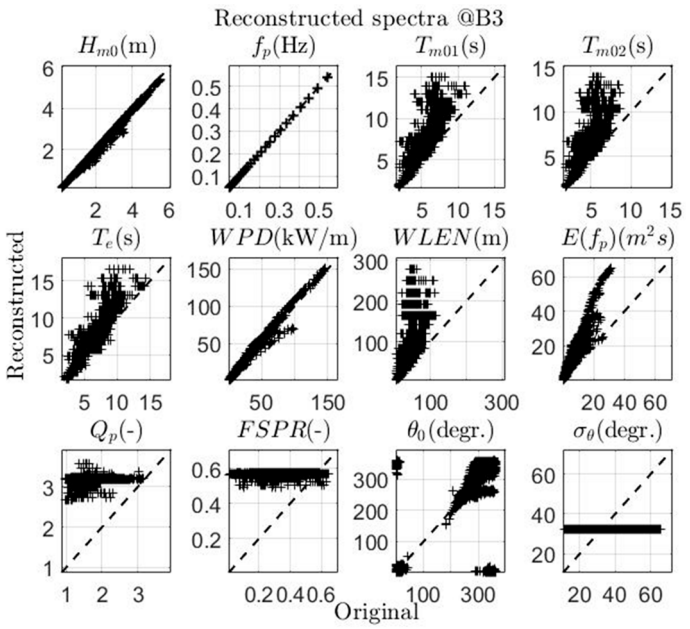

Figure S14. Scatter plots for KPs obtained from the original and the TMA–Mitsuyasu reconstructed spectra at check point B3.

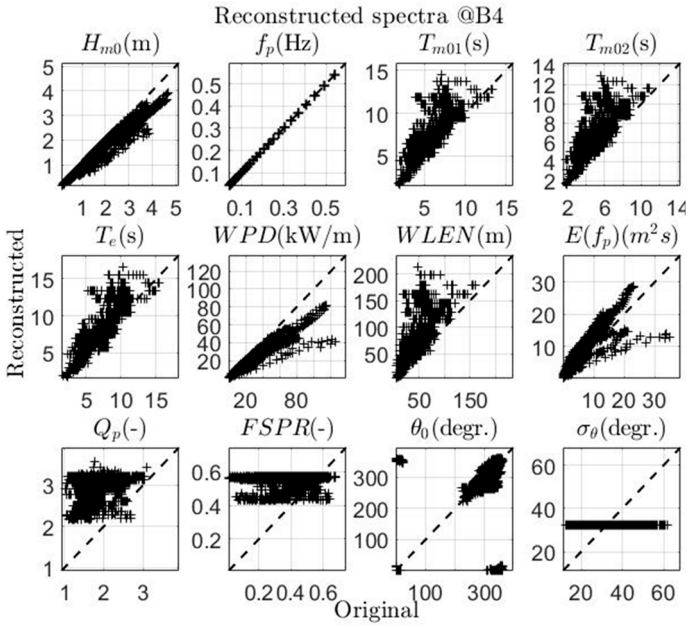

Figure S15. Scatter plots for KPs obtained from the original and the TMA–Mitsuyasu reconstructed spectra at check point B4.

Table S1. Correlation coefficient (R) of the KPs derived from the original and the reconstructed spectra/partitions at check point B1. Sample numbers of Part0 to Part6 are 8760, 6139, 8719, 3127, 1125, 384, and 109.

KPs / Part$n$	H_{m0}	f_p	T_{m01}	T_{m02}	T_e	WPD	$WLEN$	$E(f_p)$	Q_p	$FSPR$	$\theta_{0,x}$	$\theta_{0,y}$	σ_θ
Part0	1.000	0.968	0.989	0.962	0.999	1.000	0.945	0.999	0.969	0.969	0.999	0.999	0.994
Part1	1.000	1.000	0.991	0.975	0.999	1.000	0.978	0.999	0.972	0.951	0.999	0.999	0.990
Part2	1.000	1.000	0.997	0.992	0.999	1.000	0.992	0.999	0.987	0.975	0.997	0.995	0.964
Part3	1.000	1.000	0.998	0.995	0.999	1.000	0.997	0.999	0.980	0.963	0.992	0.996	0.926
Part4	1.000	1.000	0.999	0.999	0.999	1.000	0.999	1.000	0.979	0.939	0.992	0.997	0.879
Part5	1.000	0.999	1.000	0.999	1.000	1.000	1.000	1.000	0.987	0.944	0.995	0.998	0.836
Part6	1.000	1.000	0.999	0.998	1.000	1.000	0.999	0.999	0.986	0.961	0.995	0.998	0.874

Table S2. Mean absolute error (MAE) of the KPs derived from the original and the reconstructed spectra/partitions at check point B1. Sample numbers of Part0 to Part6 are 8760, 6139, 8719, 3127, 1125, 384, and 109.

KPs / Part$n$	H_{m0} (m)	f_p (Hz)	T_{m01} (s)	T_{m02} (s)	T_e (s)	WPD (kW/m)	$WLEN$ (m)	$E(f_p)$ (m^2s)	Q_p	$FSPR$	θ_0 ($degr.$)	σ_θ ($degr.$)
Part0	0	0.0012	0.1500	0.2400	0.0600	0.0900	4.1000	0.0862	0.0508	0.0164	0.8000	0.6339
Part1	0	0.0002	0.1500	0.2400	0.0500	0.0600	4.1000	0.0531	0.0715	0.0174	0.9000	0.5469
Part2	0	0.0001	0.1300	0.2100	0.0600	0.0600	4.2000	0.0552	0.1953	0.0261	2.5000	1.3501
Part3	0	0.0001	0.1200	0.1600	0.0700	0.0000	3.7000	0.0044	0.4022	0.0365	3.7000	1.5905
Part4	0	0.0001	0.0900	0.1100	0.0600	0.0000	2.8000	0.0023	0.4311	0.0368	3.7000	1.6065
Part5	0	0.0002	0.0700	0.1000	0.0500	0.0000	2.5000	0.0008	0.3872	0.0358	3.0000	1.5461
Part6	0	0.0000	0.0800	0.1100	0.0500	0.0000	2.8000	0.0006	0.3937	0.0359	3.0000	1.3737

Table S3. Correlation coefficient (R) of the KPs derived from the original and the reconstructed spectra/partitions at check point B3. Sample numbers of Part0 to Part6 are 8760, 6994, 8645, 3408, 849, 229, and 41.

KPs / Part$n$	H_{m0}	f_p	T_{m01}	T_{m02}	T_e	WPD	$WLEN$	$E(f_p)$	Q_p	$FSPR$	$\theta_{0,x}$	$\theta_{0,y}$	σ_θ

Part0	1.000	0.956	0.985	0.958	0.998	1.000	0.935	0.997	0.936	0.947	0.999	0.999	0.990
Part1	1.000	1.000	0.990	0.974	0.999	1.000	0.974	0.996	0.956	0.926	0.999	0.999	0.989
Part2	1.000	1.000	0.996	0.991	0.999	1.000	0.991	0.998	0.987	0.965	0.996	0.997	0.981
Part3	1.000	1.000	0.998	0.996	0.999	1.000	0.997	0.999	0.980	0.955	0.995	0.995	0.944
Part4	1.000	1.000	0.999	0.999	1.000	1.000	0.999	0.999	0.981	0.954	0.994	0.995	0.942
Part5	1.000	0.999	1.000	1.000	1.000	1.000	1.000	0.999	0.988	0.971	0.996	0.994	0.920
Part6	1.000	1.000	1.000	1.000	1.000	1.000	1.000	0.997	0.977	0.975	0.996	0.981	0.899

Table S4. Mean absolute error (MAE) of the KPs derived from the original and the reconstructed spectra/partitions at check point B3. Sample numbers of Part0 to Part6 are 8760, 6994, 8645, 3408, 849, 229, and 41.

KPs / Part$n$	H_{m0} (m)	f_p (Hz)	T_{m01} (s)	T_{m02} (s)	T_e (s)	WPD (kW/m)	$WLEN$ (m)	$E(f_p)$ (m^2s)	Q_p	$FSPR$	θ_0 ($degr.$)	σ_θ ($degr.$)
Part0	0	0.0017	0.1400	0.2200	0.0600	0.1000	3.5000	0.1001	0.0575	0.0190	0.9000	0.7306
Part1	0	0.0002	0.1600	0.2500	0.0600	0.0900	4.1000	0.0806	0.0739	0.0203	1.1000	0.5833
Part2	0	0.0001	0.1400	0.2100	0.0700	0.0500	4.4000	0.0427	0.2104	0.0282	2.6000	1.2632
Part3	0	0.0001	0.1200	0.1700	0.0700	0.0000	4.1000	0.0040	0.3483	0.0364	3.2000	1.4800
Part4	0	0.0001	0.0800	0.1100	0.0500	0.0000	2.5000	0.0026	0.4027	0.0317	3.2000	1.3497
Part5	0	0.0003	0.0700	0.0900	0.0400	0.0000	2.2000	0.0015	0.2959	0.0250	3.3000	1.4313
Part6	0	0.0000	0.0500	0.0700	0.0300	0.0000	1.8000	0.0020	0.3282	0.0201	3.5000	1.3780

Table S5. Correlation coefficient (R) of the KPs derived from the original and the reconstructed spectra/partitions at check point B4. Sample numbers of Part0 to Part6 are 8760, 4304, 8711, 1892, 559, 112, and 15.

KPs / Part$n$	H_{m0}	f_p	T_{m01}	T_{m02}	T_e	WPD	$WLEN$	$E(f_p)$	Q_p	$FSPR$	$\theta_{0,x}$	$\theta_{0,y}$	σ_θ
Part0	1.000	0.976	0.989	0.965	0.999	1.000	0.952	0.999	0.962	0.966	0.999	0.999	0.992
Part1	1.000	1.000	0.994	0.983	0.999	1.000	0.985	0.999	0.970	0.945	0.999	0.998	0.990
Part2	1.000	1.000	0.997	0.993	0.999	1.000	0.993	0.999	0.987	0.975	0.993	0.994	0.982
Part3	1.000	1.000	0.999	0.998	1.000	1.000	0.999	0.999	0.978	0.966	0.987	0.990	0.899
Part4	1.000	1.000	1.000	0.999	1.000	1.000	1.000	1.000	0.976	0.956	0.988	0.987	0.847
Part5	1.000	1.000	0.999	0.999	0.999	1.000	0.999	1.000	0.962	0.908	0.993	0.985	0.835
Part6	1.000	0.998	1.000	1.000	1.000	1.000	1.000	1.000	0.975	0.942	0.995	0.996	0.989

Table S6. Mean absolute error (MAE) of the KPs derived from the original and the reconstructed spectra/partitions at check point B4. Sample numbers of Part0 to Part6 are 8760, 4304, 8711, 1892, 559, 112, and 15.

KPs / Part$n$	H_{m0} (m)	f_p (Hz)	T_{m01} (s)	T_{m02} (s)	T_e (s)	WPD (kW/m)	$WLEN$ (m)	$E(f_p)$ (m^2s)	Q_p	$FSPR$	θ_0 ($degr.$)	σ_θ ($degr.$)
Part0	0	0.0011	0.1200	0.1900	0.0500	0.0600	3.1000	0.0579	0.0471	0.0150	0.8000	0.5712
Part1	0	0.0002	0.1200	0.1900	0.0500	0.0300	3.0000	0.0345	0.0721	0.0163	1.2000	0.5469
Part2	0	0.0001	0.1200	0.1800	0.0500	0.0500	3.3000	0.0446	0.1514	0.0212	2.1000	0.9332
Part3	0	0.0001	0.0900	0.1200	0.0500	0.0000	2.3000	0.0037	0.3943	0.0323	4.4000	1.8894
Part4	0	0.0001	0.0700	0.0900	0.0400	0.0000	1.9000	0.0022	0.5371	0.0355	4.4000	1.8198
Part5	0	0.0000	0.0600	0.0800	0.0500	0.0000	1.7000	0.0012	0.4753	0.0369	3.6000	1.6452
Part6	0	0.0014	0.0300	0.0400	0.0200	0.0000	0.8000	0.0005	0.2139	0.0277	4.4000	1.8823

Table S7. Correlation coefficient (R) of the KPs derived from the original and the reconstructed (obtained under different strategies of n^{fr} and n^{tl}) partitions at check point B1. The R values were derived from all the partitions identified, and the values illustrated under the other n^{fr} and n^{tl} combinations are relative to those obtained under the setting of $n^{fr} = 3$ and $n^{tl} = 6$.

KPs / n^{fr}&n^{tl}	H_{m0}	f_p	T_{m01}	T_{m02}	T_e	WPD	$WLEN$	$E(f_p)$	Q_p	$FSPR$
$n^{fr} = 3,\ n^{tl} = 6$	1	0.9996	0.9970	0.9930	0.9993	0.9999	0.9945	0.9991	0.9883	0.9765
$n^{fr} = 4,\ n^{tl} = 6$	0	-0.0008	0.0001	0.0000	0.0003	0.0000	0.0001	0.0008	0.0055	0.0123

$n^{fr} = 6,\ n^{tl} = 6$	0	-0.0010	0.0001	0.0001	0.0003	0.0000	0.0002	0.0008	0.0072	0.0137
$n^{fr} = 3\ n^{tl} = 4$	0	-0.0017	-0.0160	-0.0280	-0.0044	-0.0001	-0.0239	-0.0003	-0.0187	-0.0179
$n^{fr} = 3,\ n^{tl} = 3$	0	0.0004	-0.0252	-0.0419	-0.0080	-0.0003	-0.0347	-0.0020	-0.0277	-0.0433

Table S8. Mean absolute error (MAE) of the KPs derived from the original and the reconstructed (obtained under different strategies of n^{fr} and n^{tl}) partitions at check point B1. The MAE values were derived from all the partitions identified, and the values illustrated under the other n^{fr} and n^{tl} combinations are relative to those obtained under the setting of $n^{fr} = 3$ and $n^{tl} = 6$.

KPs / n^{fr}&n^{tl}	H_{m0} (m)	f_p (Hz)	T_{m01} (s)	T_{m02} (s)	T_e (s)	WPD (kW/m)	$WLEN$	$E(f_p)$	Q_p	$FSPR$
$n^{fr} = 3,\ n^{tl} = 6$	0	0.0001	0.1306	0.2023	0.0577	0.0426	3.9658	0.0420	0.2082	0.0259
$n^{fr} = 4,\ n^{tl} = 6$	0	0.0001	-0.0037	-0.0023	-0.0105	-0.0073	-0.0682	-0.0284	-0.0487	-0.0062
$n^{fr} = 6,\ n^{tl} = 6$	0	0.0003	-0.0036	-0.0038	-0.0083	-0.0027	-0.1443	-0.0329	-0.0978	-0.0087
$n^{fr} = 3\ n^{tl} = 4$	0	0.0004	0.2753	0.3785	0.1351	0.1682	8.3011	0.1006	0.2320	0.0101
$n^{fr} = 3,\ n^{tl} = 3$	0	-0.0001	0.3854	0.5174	0.2031	0.2438	11.3906	0.1842	0.3499	0.0238

Table S9. Correlation coefficient (R) of the KPs derived from the original and the reconstructed (obtained under different strategies of n^{fr} and n^{tl}) partitions at check point B3. The R values were derived from all the partitions identified, and the values illustrated under the other n^{fr} and n^{tl} combinations are relative to those obtained under the setting of $n^{fr} = 3$ and $n^{tl} = 6$.

KPs / n^{fr}&n^{tl}	H_{m0}	f_p	T_{m01}	T_{m02}	T_e	WPD	$WLEN$	$E(f_p)$	Q_p	$FSPR$
$n^{fr} = 3,\ n^{tl} = 6$	1	0.9997	0.9966	0.9927	0.9992	0.9998	0.9943	0.9970	0.9883	0.9714
$n^{fr} = 4,\ n^{tl} = 6$	0	-0.0012	0.0001	0.0000	0.0003	0.0000	0.0001	0.0026	0.0061	0.0164
$n^{fr} = 6,\ n^{tl} = 6$	0	-0.0007	0.0001	0.0001	0.0003	0.0000	0.0002	0.0027	0.0076	0.0183
$n^{fr} = 3\ n^{tl} = 4$	0	-0.0024	-0.0169	-0.0262	-0.0056	-0.0006	-0.0194	-0.0013	-0.0198	-0.0162
$n^{fr} = 3,\ n^{tl} = 3$	0	0.0003	-0.0331	-0.0482	-0.0130	-0.0019	-0.0358	-0.0138	-0.0350	-0.0462

Table S10. Mean absolute error (MAE) of the KPs derived from the original and the reconstructed (obtained under different strategies of n^{fr} and n^{tl}) partitions at check point B3. The MAE values were derived from all the partitions identified, and the values illustrated under the other n^{fr} and n^{tl} combinations are relative to those obtained under the setting of $n^{fr} = 3$ and $n^{tl} = 6$.

KPs / n^{fr}&n^{tl}	H_{m0} (m)	f_p (Hz)	T_{m01} (s)	T_{m02} (s)	T_e (s)	WPD (kW/m)	$WLEN$	$E(f_p)$	Q_p	$FSPR$
$n^{fr} = 3,\ n^{tl} = 6$	0	0.0001	0.1413	0.2109	0.0657	0.0499	4.1461	0.0470	0.1957	0.0269
$n^{fr} = 4,\ n^{tl} = 6$	0	0.0002	-0.0057	-0.0040	-0.0136	-0.0100	-0.1139	-0.0330	-0.0439	-0.0067
$n^{fr} = 6,\ n^{tl} = 6$	0	0.0003	-0.0058	-0.0058	-0.0112	-0.0070	-0.1939	-0.0371	-0.0861	-0.0087
$n^{fr} = 3\ n^{tl} = 4$	0	0.0005	0.2811	0.3705	0.1482	0.1472	7.9062	0.0858	0.2211	0.0084
$n^{fr} = 3,\ n^{tl} = 3$	0	-0.0001	0.4341	0.5520	0.2501	0.2864	11.7368	0.2308	0.3676	0.0285

Table S11. Correlation coefficient (R) of the KPs derived from the original and the reconstructed (obtained under different strategies of n^{fr} and n^{tl}) partitions at check point B4. The R values were derived from all the partitions identified, and the values illustrated under the other n^{fr} and n^{tl} combinations are relative to those obtained under the setting of $n^{fr} = 3$ and $n^{tl} = 6$.

KPs / n^{fr}&n^{tl}	H_{m0}	f_p	T_{m01}	T_{m02}	T_e	WPD	$WLEN$	$E(f_p)$	Q_p	$FSPR$
$n^{fr} = 3,\ n^{tl} = 6$	1	0.9996	0.9974	0.9941	0.9994	1.0000	0.9951	0.9992	0.9883	0.9788
$n^{fr} = 4,\ n^{tl} = 6$	0	-0.0006	0.0001	0.0001	0.0002	0.0000	0.0001	0.0007	0.0061	0.0109
$n^{fr} = 6,\ n^{tl} = 6$	0	-0.0007	0.0001	0.0001	0.0002	0.0000	0.0001	0.0007	0.0074	0.0123
$n^{fr} = 3\ n^{tl} = 4$	0	-0.0011	-0.0161	-0.0288	-0.0043	-0.0003	-0.0260	-0.0005	-0.0173	-0.0168
$n^{fr} = 3,\ n^{tl} = 3$	0	0.0004	-0.0282	-0.0478	-0.0087	-0.0007	-0.0446	-0.0035	-0.0256	-0.0396

Table S12. Mean absolute error (MAE) of the KPs derived from the original and the reconstructed (obtained under different strategies of n^{fr} and n^{tl}) partitions at check point B4. The MAE values were derived from all the partitions identified, and the values illustrated under the other n^{fr} and n^{tl} combinations are relative to those obtained under the setting of $n^{fr} = 3$ and $n^{tl} = 6$.

KPs / n^{fr}&n^{tl}	H_{m0} (m)	f_p (Hz)	T_{m01} (s)	T_{m02} (s)	T_e (s)	WPD (kW/m)	$WLEN$	$E(f_p)$	Q_p	$FSPR$
$n^{fr}=3,\ n^{tl}=6$	0	0.0001	0.1112	0.1730	0.0485	0.0373	3.0269	0.0350	0.1753	0.0218
$n^{fr}=4,\ n^{tl}=6$	0	0.0001	-0.0023	-0.0012	-0.0082	-0.0068	-0.0234	-0.0239	-0.0463	-0.0057
$n^{fr}=6,\ n^{tl}=6$	0	0.0002	-0.0021	-0.0023	-0.0068	-0.0044	-0.0595	-0.0279	-0.0880	-0.0074
$n^{fr}=3\ n^{tl}=4$	0	0.0004	0.2962	0.4080	0.1424	0.1931	7.7349	0.1028	0.2222	0.0088
$n^{fr}=3,\ n^{tl}=3$	0	-0.0001	0.4241	0.5668	0.2218	0.3072	10.8363	0.2074	0.3509	0.0222

Table S13. Correlation coefficient (R) of the KPs derived from the original and the reconstructed spectra (with the three and six largest partitions) at check point B1. The values of R are expressed as the differences to those obtained from the original spectra and the reconstructed ones using the four largest partitions.

KPs / Part.	H_{m0}	f_p	T_{m01}	T_{m02}	T_e	WPD	$WLEN$	$E(f_p)$	Q_p	$FSPR$	$\theta_{0,x}$	$\theta_{0,y}$	σ_θ
Largest3	0	-0.003	-0.001	-0.001	-0.001	0.000	0.000	0.000	-0.004	-0.006	0.000	-0.001	-0.004
Largest6	0	0.000	0.000	0.000	0.000	0.000	0.000	0.000	0.000	0.001	0.000	0.000	0.000

Table S14. Mean absolute error (MAE) of the KPs derived from the original and the reconstructed spectra (with the three and six largest partitions) at check point B1. The values of MAE are expressed as the differences to those obtained from the original spectra and the reconstructed ones using the four largest partitions.

KPs / Part.	H_{m0} (m)	f_p (Hz)	T_{m01} (s)	T_{m02} (s)	T_e (s)	WPD (kW/m)	$WLEN$ (m)	$E(f_p)$ (m^2s)	Q_p	$FSPR$	θ_0 ($degr.$)	σ_θ ($degr.$)
Largest3	0	0.000	0.010	0.000	0.010	0.010	0.100	0.002	0.003	0.001	0.100	0.119
Largest6	0	0.000	0.000	0.000	0.000	0.000	0.000	0.000	0.000	0.000	0.000	-0.009

Table S15. Correlation coefficient (R) of the KPs derived from the original and the reconstructed spectra (with the three and six largest partitions) at check point B3. The values of R are expressed as the differences to those obtained from the original spectra and the reconstructed ones using the four largest partitions.

KPs / Part.	H_{m0}	f_p	T_{m01}	T_{m02}	T_e	WPD	$WLEN$	$E(f_p)$	Q_p	$FSPR$	$\theta_{0,x}$	$\theta_{0,y}$	σ_θ
Largest3	0	-0.003	-0.001	-0.001	-0.001	0.000	-0.001	0.000	-0.004	-0.005	0.000	-0.001	-0.005
Largest6	0	0.000	0.000	0.000	0.000	0.000	0.000	0.000	0.000	0.001	0.000	0.000	0.000

Table S16. Mean absolute error (MAE) of the KPs derived from the original and the reconstructed spectra (with the three and six largest partitions) at check point B3. The values of MAE are expressed as the differences to those obtained from the original spectra and the reconstructed ones using the four largest partitions.

KPs / Part.	H_{m0} (m)	f_p (Hz)	T_{m01} (s)	T_{m02} (s)	T_e (s)	WPD (kW/m)	$WLEN$ (m)	$E(f_p)$ (m^2s)	Q_p	$FSPR$	θ_0 ($degr.$)	σ_θ ($degr.$)
Largest3	0	0.000	0.010	0.000	0.010	0.010	0.100	0.003	0.003	0.001	0.100	0.080
Largest6	0	0.000	0.000	0.000	0.000	0.000	0.000	0.000	0.000	0.000	0.000	-0.004

Table S17. Correlation coefficient (R) of the KPs derived from the original and the reconstructed spectra (with the three and six largest partitions) at check point B4. The values of R are expressed as the differences to those obtained from the original spectra and the reconstructed ones using the four largest partitions.

KPs / Part.	H_{m0}	f_p	T_{m01}	T_{m02}	T_e	WPD	$WLEN$	$E(f_p)$	Q_p	$FSPR$	$\theta_{0,x}$	$\theta_{0,y}$	σ_θ
Largest3	0	-0.005	0.000	0.000	0.000	0.000	0.000	0.000	-0.001	-0.003	0.000	0.000	-0.002
Largest6	0	0.000	0.000	0.000	0.000	0.000	0.000	0.000	0.000	0.000	0.000	0.000	0.000

Table S18. Mean absolute error (MAE) of the KPs derived from the original and the reconstructed spectra (with the three and six largest partitions) at check point B4. The values of MAE are expressed as the differences to those obtained from the original spectra and the reconstructed ones using the four largest partitions.

KPs / Part.	H_{m0} (m)	f_p (Hz)	T_{m01} (s)	T_{m02} (s)	T_e (s)	WPD (kW/m)	$WLEN$ (m)	$E(f_p)$ $(m^2 s)$	Q_p	$FSPR$	θ_0 $(degr.)$	σ_θ $(degr.)$
Largest3	0	0.000	0.000	0.000	0.000	0.000	0.000	0.002	0.001	0.001	0.100	0.042
Largest6	0	0.000	0.000	0.000	0.000	0.000	0.000	0.000	0.000	0.000	0.000	-0.004